Cell PRESS
Structure
Article

Structure of *Arabidopsis* HYPONASTIC LEAVES1 and Its Molecular Implications for miRNA Processing

Seong Wook Yang,[1,2,5] Hong-Ying Chen,[1,5] Jing Yang,[3,4] Satoru Machida,[3,4] Nam-Hai Chua,[2,*] and Y. Adam Yuan[3,4,*]
[1]Host-Pathogen Interaction Group, Temasek Life Sciences Laboratory, National University of Singapore, 1 Research Link, Singapore 117604, Singapore
[2]Laboratory of Plant Molecular Biology, The Rockefeller University, New York, NY 10065, USA
[3]Department of Biological Sciences, National University of Singapore, 14 Science Drive 4, Singapore 117543, Singapore
[4]Structural Biology Group, Temasek Life Sciences Laboratory, National University of Singapore, 1 Research Link, Singapore 117604, Singapore
[5]These authors contributed equally to this work
*Correspondence: chua@mail.rockefeller.edu (N.-H.C.), adam@tll.org.sg (Y.A.Y.)
DOI 10.1016/j.str.2010.02.006

SUMMARY

The *Arabidopsis* HYPONASTIC LEAVES1 (HYL1) is a double-stranded RNA-binding protein that forms a complex with DICER-LIKE1 (DCL1) and SERRATE to facilitate processing of primary miRNAs into microRNAs (miRNAs). However, the structural mechanisms of miRNA maturation by this complex are poorly understood. Here, we present the crystal structures of double-stranded RNA binding domains (dsRBD1 and dsRBD2) of HYL1 and HYL1 dsRBD1 (HR1)/dsRNA complex as well as human TRBP2 dsRBD2 (TR2)/dsRNA complex for comparison analysis. Structural and functional study demonstrates that both HR1 and TR2 are canonical dsRBDs for dsRNA binding, whereas HR2 of HYL1 is a noncanonical dsRBD harboring a putative dimerization interface. Domain swapping within the context of HYL1 demonstrates that TR2 can supplant the function of HR1 in vitro and in vivo. Further biochemical analyses suggest that HYL1 probably binds to the miRNA/miRNA* region of precursors as a dimer mediated by HR2.

INTRODUCTION

MicroRNAs (miRNA) have recently emerged to be important regulators of gene expression through their action on sequence-specific repression of mRNA translation and degradation (reviewed by Siomi and Siomi, 2009). A miRNA gene is initially transcribed by RNA polymerase II as a long primary transcript [primary miRNA (pri-miRNA)], which is subsequently processed to precursor miRNA (pre-miRNA) with stem loops; pre-miRNA is then cleaved into ~21 nt mature miRNA by RNase III family nucleases (reviewed by Jaskiewicz and Filipowicz, 2008; Ji, 2008). The mature miRNA is loaded into RNA induced silencing complex to pair with target mRNAs for mRNA cleavage or translational inhibition (reviewed by Hutvágner and Simard, 2008; Jinek and Doudna, 2009). Notably, there are significant differences in first steps in pri-miRNA processing between plants and animals.

In animal cells, pri-miRNA processing is clearly separated from pre-miRNA processing in time, components of the processing complex, and their cellular locations. pri-miRNA is first processed to pre-miRNA by a complex of two proteins, Drosha, an RNase III protein, and DIGEORGE SYNDROME CRITICAL REGION GENE 8 (DGCR8), a dsRNA-binding protein (Han et al., 2004a, 2006; Landthaler et al., 2004) inside the nucleus. The resulting pre-miRNA is then cleaved to mature miRNA/miRNA* duplex by another RNase III protein, Dicer, assisted by dsRNA-binding proteins (Hutvágner et al., 2001; Chendrimada et al., 2005) in the cytoplasm.

Studies in the last few years have uncovered critical roles of double-stranded RNA-binding proteins in facilitating pri-miRNA/pre-miRNA processing by RNase III family nucleases in several organisms (Collins and Cheng, 2005). For example, the *Drosophila* Loquacious protein, which contains three tandem double-stranded RNA binding domains (dsRBDs), works in concert with DICER1 to convert pre-miRNAs into miRNA/miRNA* duplexes (Förstemann et al., 2005; Saito et al., 2005; Jiang et al., 2005), whereas R2D2 protein, which contains two tandem dsRBDs, functions along with DICER2 to detect the differential stability of siRNA duplex ends and determine which strand enters RNA induced silencing complex (Liu et al., 2003; Tomari et al., 2004, 2007). The human DGCR8 harboring two tandem dsRBDs associates with Drosha to convert pri-miRNAs into pre-miRNAs (Han et al., 2004a, 2006; Landthaler et al., 2004), whereas TAR (HIV-1) RNA BINDING PROTEIN 2 (TRBP2) harboring three tandem dsRBDs recruits the Dicer complex to Ago2 for miRNA processing (Chendrimada et al., 2005). Moreover, the Dicer-TRBP2 complex is sufficient to process pre-miRNA into miRNA as well as long dsRNA into siRNA (Chendrimada et al., 2005).

The human DGCR8 is thought to show preferential binding to the junction between the double-stranded RNA stem portion and the single-stranded flanking fragment of pri-miRNA. Upon binding, this protein presumably serves as a molecular ruler to recruit Drosha for precise cleavage of pri-miRNA ~11 bp away from the junction (Han et al., 2006). Recent crystal structure of the DGCR8 core domain containing two tandem dsRBDs shows that it is sufficient to serve as a molecular ruler, although the core

domain primarily binds to the dsRNA stem region of pri-miRNA and does not preferentially recognize the junction (Sohn et al., 2007).

In plants, both pri-miRNA processing and pre-miRNA processing occur inside the nucleus by a complex comprising of at least three protein subunits: DCL1 (an RNase III protein), HYL1 (a dsRNA-binding protein), and SERRATE (SE; a zinc-finger-domain protein). These three proteins are all required for the maturation of miRNA/miRNA* duplexes from plant pri-miRNAs (Grigg et al., 2005; Kurihara et al., 2006; Lobbes et al., 2006; Dong et al., 2008). As in animal cells where dsRNA-binding protein DGCR8 and TRBP2 are essential factors for miRNA processing, the *Arabidopsis* dsRNA-binding protein HYL1 plays a critical role in assisting DCL1 in the precise processing of miRNAs from pri-miRNAs (Kurihara et al., 2006). HYL1 contains two tandem dsRBDs, a putative nuclear localization signal at its N terminus and a putative protein-protein interaction domain at its C terminus (Lu and Fedoroff, 2000; Han et al., 2004b). The HYL1 C-terminal domain appears to be dispensable for function and the N-terminal region containing the two tandem dsRBDs alone is sufficient to completely rescue the *hyl1-2* phenotype (Wu et al., 2007). In vitro miRNA processing assays using recombinant DCL1, HYL1, and SE demonstrated that both HYL1 and SE are functional components of a complex that are required for precise and efficient processing of miRNAs from pri-miRNAs (Dong et al., 2008).

Because the N-terminal HYL1 fragment comprising two tandem dsRBDs can facilitate pri-miRNA cleavage by DCL1, it is reasonable to assume that dsRNA binding proteins may possess a general mechanism to recognize pri-miRNA and present the latter for cleavage by RNase III enzymes. To investigate the structural basis for miRNA precursor recognition, we have determined the crystal structures of individual HYL1 dsRBD domains (dsRBD1or HR1 and dsRBD2 or HR2) and HR1/dsRNA complex as well as human TRBP2 RBD2/dsRNA (TR2/dsRNA) complex for comparative analysis.

Analysis by electrophoretic mobility shift assays (EMSA) demonstrated that HR1 as well as TR2 possess high dsRNA binding affinity, which is greatly reduced in HR2. Consistent with the EMSA results, domain swapping experiments showed that TR2 is capable of replacing HR1 both in vitro and in vivo: TR2+HR2 chimeric protein has similar pri-miRNA binding affinity in vitro compared with HR1+2 and the TR2+HR2 chimeric protein is able to rescue the *hyl1-2* mutant phenotype in vivo. Notably, from the crystal structure we found HR2 harbors a putative dimerization interface. The dimerization of HYL1 was further confirmed by in vitro pull-down, coimmunoprecipitation, and analytical gel filtration assays.

On the basis of these structural, biochemical, and in vivo analyses, we propose a hypothetical model for HYL1/dsRNA interaction. Our model suggests that HR1 and HR2 may function cooperatively for dsRNA binding, whereas HR2 may further mediate HYL1 dimerization to strengthen dsRNA binding affinity and enable HYL1 to scan along pri-miRNA/pre-miRNA to preferentially recognize the miRNA/miRNA* region or thermodynamically stable stem region of pri-miRNA. Working together with SE, HYL probably serves as a molecular ruler to facilitate precise and efficient miRNA processing by DCL1.

RESULTS

Crystal Structures of Double-Stranded RNA Binding Domains

To investigate the structural principles for recognition of miRNA precursors by *Arabidopsis* HYL1, we have screened hundreds of cocrystallization conditions of HYL1 and its fragments with a series of RNA duplexes of different lengths. At the end, we were able to crystallize and determine the crystal structures of individual dsRBDs of HYL1 (HR1 and HR2) and of HR1/dsRNA complex (two 10 bp dsRNA stacked collinearly) (Figure 1A). For comparative purpose we also determined the crystal structure of the human TR2/dsRNA complex (two 10 bp dsRNA stacked collinearly). All these structures were determined by molecular replacement using the crystal structure of the second dsRBD of *Xenopus laevis* RNA-binding protein A as the search model (PDBID: 1DI2). The latter was cocrystallized with the similar 10 bp RNA duplex, which we used for cocrystallizations of HR1 and TR2 (Ryter and Schultz, 1998). Crystallographic statistics are summarized in Table 1.

Like other dsRBDs (reviewed by Doyle and Jantsch, 2002), HR1, HR2, and TR2 are approximately 70 amino acids in length and share the similar overall fold with a common α-β-β-β-α structure in which the two α helices lie on the surface of a three-stranded anti-parallel β sheet (Figure 1B; see Figure S1 available online). Comparison of crystal structures of the dsRBDs with the search model *Xenopus laevis* dsRBD2 shows that HR1, HR2, and TR2 have rmsd values of 3.046 Å, 3.033 Å, and 0.658 Å (68 Cα atoms), respectively (Figure 1C). Therefore, the structures of TR2 are much closer to those of *Xenopus laevis* dsRBD2, which binds to the dsRNA (Ryter and Schultz, 1998). Although HR1 and HR2 have a similar fold with an rmsd value of 2.865 Å (68 Cα atoms), there are significant structural deviations between them at the putative RNA binding surfaces. HR1 has close structural similarities with the human TR2 and *Xenopus laevis* dsRBD2 in these regions, including region 2, which contains the invariable histidine residue (Figure 1B). In contrast, HR2 has less structural similarity in these regions, including the different loop orientation at region 2 and an $\sim$3.5 Å helix movement toward the potentially bound dsRNA in region 1 (Figure 1C). Since neither the loop at region 2 nor the α helix at region 1 is heavily involved in protein-protein packing in the crystal, the significant structural deviation of HR2 from other consensus dsRBD at the putative dsRNA binding surface (Figure 1D) strongly suggests that HR2 is unable to bind canonical dsRNA.

DsRNA Binding Surface versus Dimerization Interface

Comparison of crystal structures of HR1/dsRNA complex and TR2/dsRNA complex with the crystal structure of *Xenopus laevis* dsRBD2/dsRNA complex reveals a conserved dsRNA binding surface with a similar electrostatic potential charge distribution (Figures 2A, 2C, and 2D). All these canonical dsRBDs share a conserved positive electrostatic potential charge in region 3, which is involved in recognizing the major groove of dsRNA. Similar neutral or slightly negative electrostatic potential surfaces in region 1 and region 2, together with a small patch of a positive electrostatic potential surface in region 2, which contains the invariable histidine residue, specifically recognize

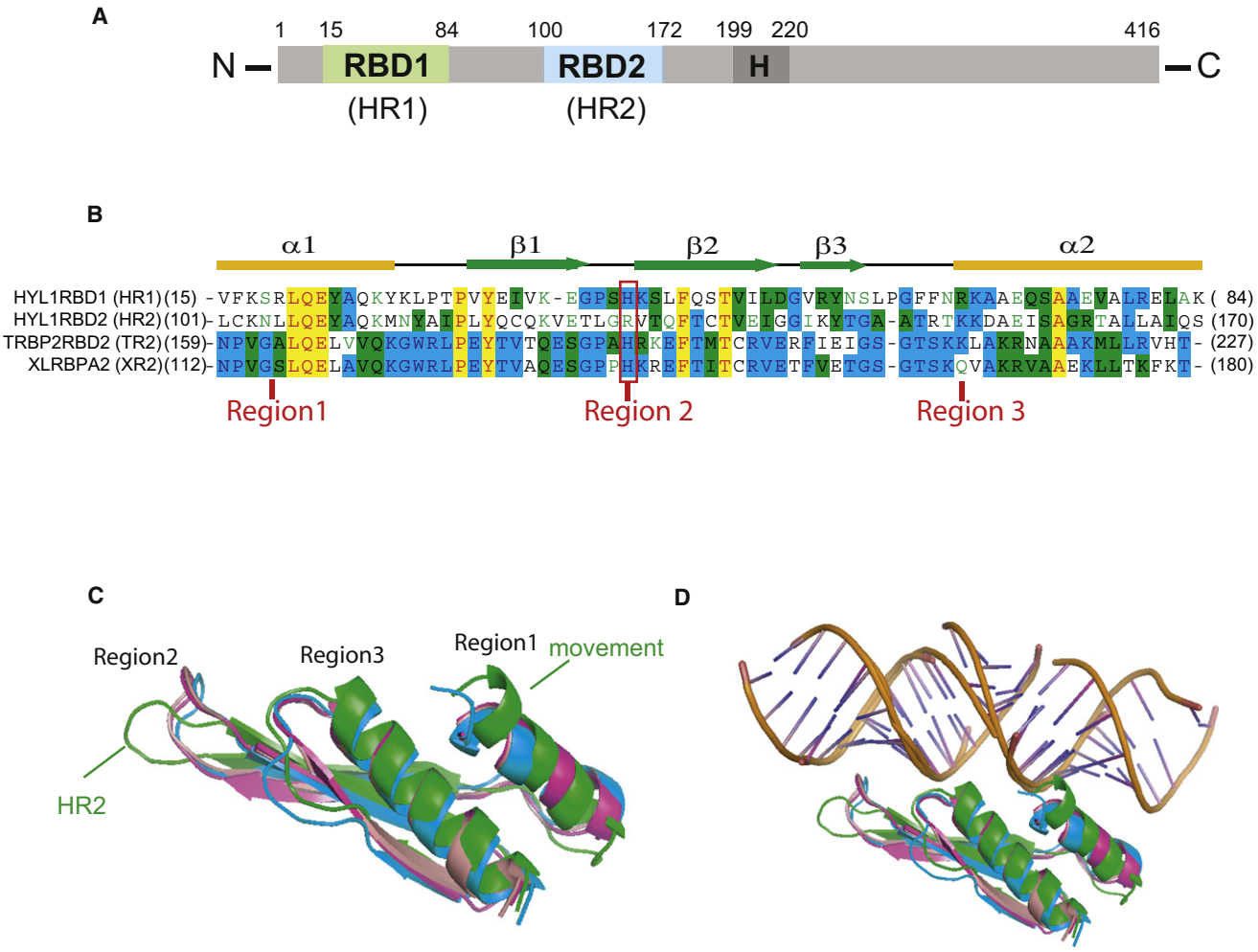

Figure 1. Domain Architecture, Sequence Alignment, and Overall Structure of and Structural Comparison of Different dsRBDs

(A) Schematic of the dsRBD domain borders in *Arabidopsis* HYL1.

(B) Sequence alignment and secondary structures of four different dsRBDs. The aligned sequences are in the order of HR1, HR2, TRBP2 dsRBD2 (TR2), and XLRBPA dsRBD2 (XR2). The secondary structure diagram for dsRBD is shown on the top. The α helices are colored in yellow and β strands in green. Conserved residues are shaded in cyan (80% conservation) and green (60% conservation), whereas essentially invariant residues are shaded in yellow. The invariable histidine residues within canonical dsRBDs are highlighted by a red rectangle and three regions involved in dsRNA recognition are indicated.

(C and D) Significant secondary structural differences between HR2 (green) and other dsRBDs. Note the different orientation of the recognition loop in region 2 and ~3.5 Å movement toward the putative bound dsRNA at region 1 (C), which disrupts the dsRNA binding (D). HR1 is shown in blue, HR2 in green, TR2 in magenta, and XR2 in pink.

the dsRNA minor groove. These canonical dsRBDs recognize two successive minor grooves and the intervening major groove within an RNA duplex with a total of ~16 bp in length formed by two stacking GC-rich dsRNA (Figures 2A, 2C, and 2D).

To determine whether the conserved residues observed in the interaction with dsRNA play a primary role in dsRNA binding, we introduced point mutations on the conserved residues H43 (region 2) and R67 (region 3) to yield HYL1 H43A and HYL1 R67A mutants. EMSA analysis showed that both HYL1 H43A and HYL1 R67A mutants displayed only slightly decreased dsRNA binding affinity, whereas the negative control mutants, HYL1 R19A, HYL1 R19K, and HYL1 Q21A, showed similar dsRNA binding affinity compared to the wild-type (WT) HYL1 (Figure S2). The marginal decrease in binding affinity observed with HYL1 mutants is not surprising since we found that canonical dsRBDs interact extensively with dsRNA. This notion is consistent with the recent report that multiple mutations on the DGCR8 core had no detectable effect on dsRNA binding affinity (Sohn et al., 2007). Interestingly, point mutations at the third dsRBD domain of *Drosophila* staufen lead a significant decrease of dsRNA binding affinity, probably due to the unique RNA stem loop binding mode exhibited by this dsRBD domain (Ramos et al., 2000).

In contrast, comparison of HR2 with HR1 reveals significant structural differences at the putative dsRNA binding regions 2 and 3 of HR2. HR2 contains a somehow different orientation of the loop at region 2 with the conserved histidine residue for minor groove recognition being replaced by an arginine residue (Figures 1B and 1C). The non-canonical HR2 has a significantly different electrostatic potential surface in region 2, with a big

Table 1. Data Collection and Refinement Statistics

	HYL1 dsRBD1	HYL1 dsRBD1/ dsRNA	HYL1 dsRBD2	TRBP2 dsRBD2/ dsRNA
PDBID	3ADG	3ADI	3ADJ	3ADL
Space group	$P2_12_12_1$	$P4_3$	$P4_3$	$I2_12_12_1$
Cell dimensions				
a (Å)	36.39	47.62	46.11	55.30
b (Å)	37.90	47.62	46.11	60.43
c (Å)	51.26	115.38	33.32	99.89
Protein molecules/ASU	1	3	1	1
Wavelength (Å)	1.54	1.54	1.54	1.10
Resolution (Å)[a]	1.7	3.2	3.0	2.2
R_{sym} (%)[a]	3.2 (18.2)	10.1 (46.7)	5.6 (25.0)	4.6 (29.3)
$I/\sigma(I)$	40.0 (9.0)	19.9 (4.7)	38.6 (8.1)	54.0 (10.1)
Completeness (%)[a]	98.4 (97.4)	97.9 (97.5)	99.7 (97.9)	99.1 (98.1)
Redundancy	5.7	7.7	7.0	14.4
Resolution (Å)	1.7	3.2	3.0	2.2
No. reflections	7709	3783	1322	8276
R_{work} (R_{free}) (%)	20.7 (25.4)	20.4 (31.7)	25.5 (32.2)	26.1 (29.8)
No. atoms				
Protein	579	1,716	547	596
Ligand/ion		422		430
Water	124		5	47
B factors (Å^2)				
Protein	30.22	69.66	30.80	48.24
Ligand/ion		60.70		45.07
Water	34.86		41.35	59.28
Rmsd				
Bond lengths (Å)	0.016	0.011	0.017	0.012
Bond angles (°)	1.376	1.619	1.627	1.492

[a] Values for the highest-resolution shell are in parentheses.

patch of strong negatively charged surface adjacent to a patch of positively charged surface (Figure 2B). There is also a distinct difference in the surface shape of region 2 of HR2. Canonical dsRBDs have two protruding edges in region 2 for dsRNA recognition, whereas HR2 has no such protruding edge in the same region (Figures 2A, 2C, and 2D). The charge and shape differences as well as the change at the conserved histidine residue in region 2 render HR2 unlikely to bind to a canonical dsRNA. On the other hand, the partially merged positively charged surface in regions 2 and 3 provides an extended positively charged surface for HR2 to potentially recognize partner proteins bearing negatively charge surfaces. The significant deviation of the potential charge and surface shape of the putative dsRNA binding surface of HR2 suggests that this surface may mediate protein-protein interaction rather than dsRNA binding (Figure 2B). Indeed, our structural analysis of HR2 domain uncovers a putative dimerization interface. This dimerization interface is primarily formed between the β1 strand of one HYL1 dsRBD2 molecule and the β3′ strand of its symmetric related molecule in a parallel interaction mode, whereas the C-terminal α2′ from the symmetric related molecule resides on the top of the β sheet formed by β1 and β2 (Figure 2E). The dimerization interface buries ~1,460 Å^2 of the total solvent-accessible area per molecule with perfectly complementary electrostatic potential interactions (Figures 2B and 2F), suggesting that this dimerization interface has biological significance and is not an artifact of crystal packing. Our structural observation is consistent with the report that many non-canonical dsRBDs are able to form a homodimer independently of the presence of dsRNA (Doyle and Jantsch, 2002).

Next, we tested whether point mutations at the dimeric surface of HR2 can disrupt HR2 dimerization. To this end, we made eight triple mutants, namely, Y120A/Q121A/C122A, L128A/G129A/R130A, K144A/Y145A/T146A, and T152A/K153A/K154A, within the context of HR1+2 or HR2, respectively. However, all of these triple mutants yield misfolded proteins or no protein expression at all. Hence, in spite of extensive efforts, we failed to generate mutations at the putative dimerization interface, which can significantly disrupt dimerization without changing the overall fold of HR1+2 or HR2.

HYL1 Has No Binding Preference for miRNA Precursors Other Than miRNA/miRNA* Duplex

To investigate the molecular mechanism for miRNA precursors binding by HYL1, we constructed cDNAs encoding full-length HYL1 and a series of HYL1 deletion mutants for in vitro RNA binding assays using pri-miRNA, pre-miRNA, and siRNA duplexes as substrates. Figure 3A shows that full-length HYL1 was able to interact with in vitro transcribed pri-miR164b to form a stable HYL1-RNA complex and the amount of protein-RNA complex increased with increasing amounts of HYL1 protein. This result is consistent with the recent report that HYL1 is able to pull down miRNA precursors by immunoprecipitation (Song et al., 2007). Furthermore, the stable HYL1-pri-miR164b complex can be competed by either pre-miR164b or 21-nt (19 bp duplex) miR164b/*, suggesting that HYL1 has no apparent binding preference for miRNA precursors other than miRNA/miRNA* duplex (Figure 3A, left). Because pri-miRNAs, pre-miRNAs, and miRNAs/* duplexes are produced by sequential steps of the miRNA biogenesis pathway, the ability of HYL1 to bind to all these RNAs may suggest that HYL1 possibly participates in several sequential steps during miRNA processing and maturation.

To further investigate functional roles of individual dsRBD domains of HYL1 and confirm our structural findings that HR1 is a canonical dsRBD whereas HR2 is a non-canonical dsRBD, we performed EMSA on HYL1 and HR1 and HR2 using pre-miR164b as an RNA substrate (Figure 3A, right). HR1 displayed low binding affinity with pre-miR164b compared with full-length HYL1, HYL1 core (HR1+2), and HYL1 core extension (HR1+2+H) in spite of the fact that HR1 is the only canonical dsRNA binding domain within the protein. In contrast, HR2 displays very weak binding affinity with pre-miR164b. Using EMSA, we estimated that full-length HYL1 displayed a 40-fold higher binding affinity than HR1 for dsRNA (Figure S3A), which suggests that HR1 is necessary for dsRNA interaction but insufficient for high binding affinity. This surprising difference of dsRNA binding affinity between full-length HYL1 and HR1 also suggests that HR2 may be involved in dsRNA binding enhancement.

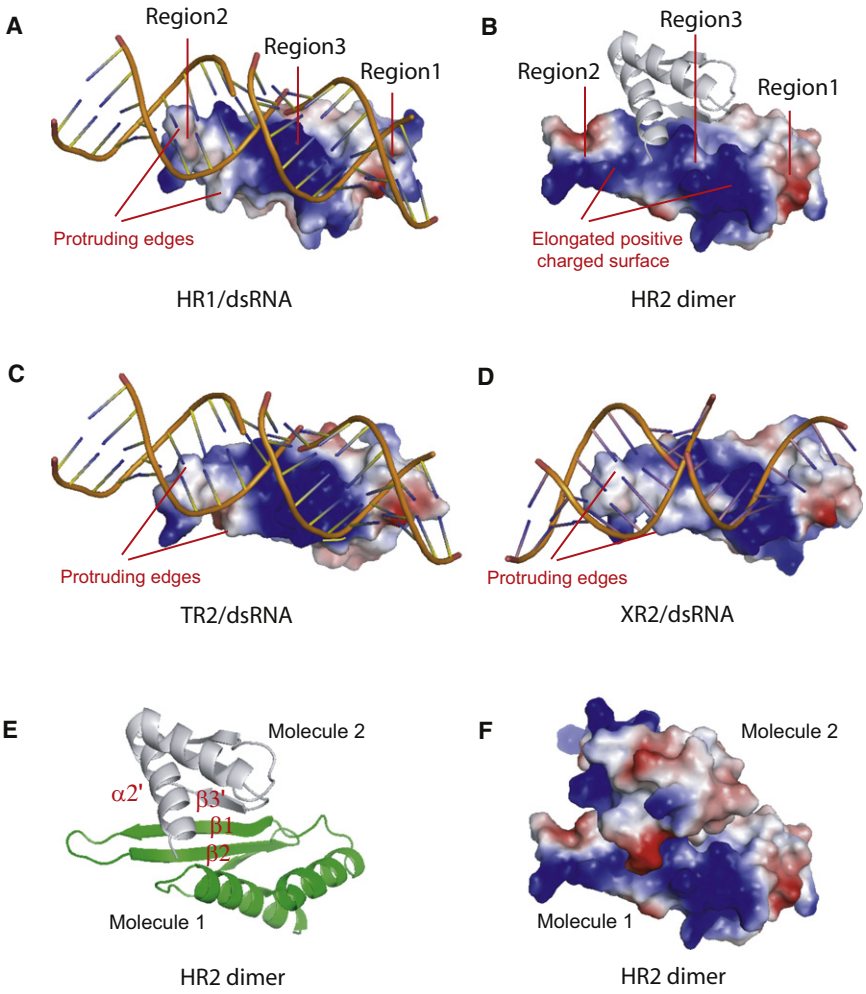

Figure 2. DsRNA or Protein Binding Surfaces of Individual dsRBDs

(A–D) Electrostatic potential views of individual dsRBDs bound to dsRNA or partner protein. Note that HR1 (A), TR2 (C), and XR2 (D) are canonical dsRNA binding domains with the bound dsRNA being recognized by two protruding edges, whereas HR2 is a non-canonical dsRNA binding domain with the partner protein being recognized by the elongated positive electrostatic potential charged surface. Individual dsRBDs are represented as electrostatic potential view and bound dsRNA and protein partner are represented as ribbon view with the blue, red, and white colors representing the positive, negative, and neutral charge, respectively. The protruding edges for dsRNA recognition and the elongated positive charged surface are indicated. Three regions involved in dsRNA recognition are also shown.

(E) Ribbon representation of HR2 dimer. The dimerization interface is primarily formed between the β1 strand of one HR2 molecule and the β3′ strand of its partner molecule in a parallel interaction mode, whereas the C-terminal α2′ from the partner molecule is located on top of the β sheets formed by β1 and β2.

(F) Electrostatic potential charge representation of HR2 dimer with the same orientation as in (B). The dimerization interface buries ~1460 Å^2 of total solvent-accessible area per molecule with perfectly complementary electrostatic potential interactions.

HYL1 Probably Recognizes the Configuration of dsRNA Secondary Structure

Plant pri-miRNAs have various lengths of stem and loop structures with the ~21 bp miRNA/miRNA*s embedded within the folded pre-miRNAs. The distinct binding affinity between HYL1 and pre-miRNAs raised the question how HYL1 distinguishes the miRNA/miRNA* region from the non-miRNA duplex regions within a folded pre-miRNA. Because HYL1 did not exhibit apparently sequence-specific dsRNA binding (data not shown), we speculated that secondary structures of dsRNAs might determine HYL1-dsRNA interaction. To investigate this hypothesis, we conducted EMSA using four non-miRNA 21 nt (19 bp) duplexes from proximal regions of miR160/* or miR164/* (Figure S4 and Table S2). Our EMSA data showed that 21 nt (19 bp) duplexes from proximal regions of miR160/* or miR164/* in miRNA precursors displayed reduced HYL1 binding affinity, although these duplexes possess similar dsRNA lengths as those of miR160/* or miR164/* (Figure 3B, top panel, with the secondary structure shown at Figure 3C). The situation was also applied to HYL1 core domain (HR1+2) (Figure 3B, bottom).

Taken together, these results suggest that configuration of dsRNA secondary structure is probably an important determinant for HYL1/dsRNA interaction mediated by HR1+2 core domain, consistent with the structural findings that canonical dsRBDs have the preference to bind to the standard RNA duplexes without significant bending (Figures 2A and 2C).

TR2+HR2 Chimeric Protein Can Replace HR1+2 Core Domain In Vitro and In Vivo

Our biochemical analysis showed that HR1+2 core domain plays an important role in the maturation of miRNA from precursors by recognizing the miRNA/miRNA* region in a sequence-independent mode. If HR1+2 core domain can indeed participate in distinguishing the miRNA/miRNA* region within precursors through scanning of the secondary structure of miRNA/miRNA*, its function may be supplanted by other dsRNA-binding domains comprising a similar domain arrangement. To this end, we tested whether TR2 can replace HR1 in the context of HYL1 to fulfill HYL1 biological functions both in vitro and in vivo given the closely structural and functional similarities between TR2 and HR1 (Figures 2A and 2C) (Daviet et al., 2000). As expected, chimeric TR2+HR2 and HR1+2 bind to miR160/* with similar high affinity (K_d = 7.8 ± 0.52 × 10^{-8} M versus K_d = 7.6 ± 0.48 × 10^{-8} M) (Figure 4A; Figure S3B), which suggests that the TR2 domain is able to functionally supplant the HR1 domain in miRNA/miRNA* binding in vitro.

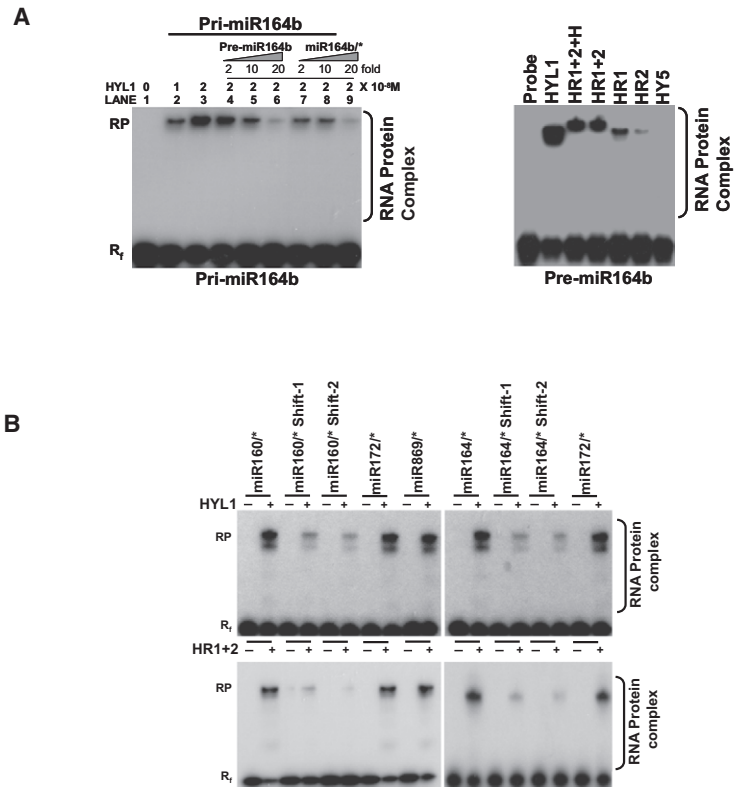

Figure 3. Gel Mobility Shift Assay of HYL1 with Pri-miRNA, Pre-miRNA, 21 nt (19 bp Duplex) miRNA/miRNA*, and Non-miRNA/miRNA* Duplexes

(A) (Left) Interaction of HYL1 with pri-miRNA. Full-length HYL1 was added to each reaction in the indicated amounts (0–2 × 10^{-8} M). Lanes 1–3, 2 × 10^{-8} M of ^{32}P-labeled pri-miRNA164b was used as probe; lanes 4–6, same as lane 3 but with increasing amounts of unlabelled pre-miRNA164b; lanes 7–9, same as lane 3 but with increasing amounts of unlabelled 21 nt (19 bp duplex) miRNA164/*. (Right) Interaction of HYL1 with pre-miRNA. Varying amounts (HYL1, 2 × 10^{-8} M; HR1+2+H, 2 × 10^{-8} M; HR1+2, 2 × 10^{-8} M; HR1, 2 × 10^{-7} M; HR2, 2 × 10^{-6} M) of HYL1 deletion mutants were added to each reaction with 2 × 10^{-8}M of ^{32}P-labeled pre-miRNA164b.

(B) Interaction of HYL1 with non-miRNA sequences in the stem and loop regions of miRNA precursors. (Top) Full-length HYL1 protein (2 × 10^{-8} M) was incubated with four different non-miRNA duplex probes (2 × 10^{-8} M): 21 nt miR160/* shift-1, 21 nt miR160/* shift-2, 21 nt miR164/* shift-1, and 21nt miR164/* shift-2. These probes contain more internal loops, unpaired bases, and mismatches compared with miRNA160/* or miR164/*. MiR172/* and miR869/* were used as positive controls. (Bottom) HR1+2 core domain of HYL1 protein (4 × 10^{-8} M) was incubated with four different non-miRNA duplex probes (2 × 10^{-8} M).

(C) Secondary structures of non-miRNA/miRNA*, miR160/miR160*, and miR164/miR164* duplexes used in gel mobility shift assays.

Since chimeric TR2+HR2 efficiently bound to duplex miR160/* with an affinity similar to that of HR1+2, we generated transgenic lines in the *hyl1-2* mutant background to assess the in vivo function of TR2+HR2. Consistent with its in vitro activity, chimeric TR2+HR2 can rescue the miRNA-deficient phenotype of the *hyl1-2* mutant to a large extent (Figures 4B and 4C). Typical phenotypes of *hyl1-2* such as upward curling leaf shape, relatively small plant size, small curled silique, and abnormal influorescence and flowers were relatively complemented to WT-like phenotypes by expression of TR2+HR2. Along with the recovery of WT morphology, miRNA deficiencies and target mRNA levels of *hyl1-2* mutant were also restored to close to WT expression levels (Figures 4D and 4E). These molecular and morphological results support the notion that TR2+HR2 can largely restore HYL1 deficiency in the *hyl1-2* mutant background and its activity is comparable to that of HR1+2 (Wu et al., 2007).

To investigate whether chimeric TR2+HR2 also has the same function as HR1+2 in upstream miRNA processing, we conducted coimmunoprecipitation of miRNA precursor using anti-HYL1 antibody. Indeed, miR164b and miR172a precursors were detected from the extract prepared from chimeric TR2+HR2-rescued *hyl1-2* in immunocomplexes, whereas no miRNA precursors were found in extract prepared from *hyl1-2*. Similar experiments using WT (Col-0) and *se-1* and *dcl1-9* mutant plants showed that pre-miRNA binding to HYL1 did not require SE or DCL1 (Figure 4F).

HYL1 May Recognize 21nt dsRNA as a Dimer

As the exact size of HYL1-dsRNA complexes could not be inferred by in vitro pull-down assays and in vivo immunoprecipitation, we attempted to determine the size of the complex by gel filtration. Freshly purified full-length HYL1 is monomeric but multimerization occurred after prolonged incubation of the protein without 21 nt dsRNA (Figure 5A). The spontaneously formed multimeric protein complexes are around 440 kDa, equal to eight to ten molecules of HYL1, whereas the HYL1 monomer peak is observed between 67 kDa and 43 kDa, consistent with the expected size (46 kDa) of the protein. A short incubation of HYL1 with 21 nt dsRNA shifted 90% of the HYL1 monomer peak to a peak of 110 kDa (Figure 5B), corresponding approximately to the combined mass of two HYL1 and one 21 nt dsRNA

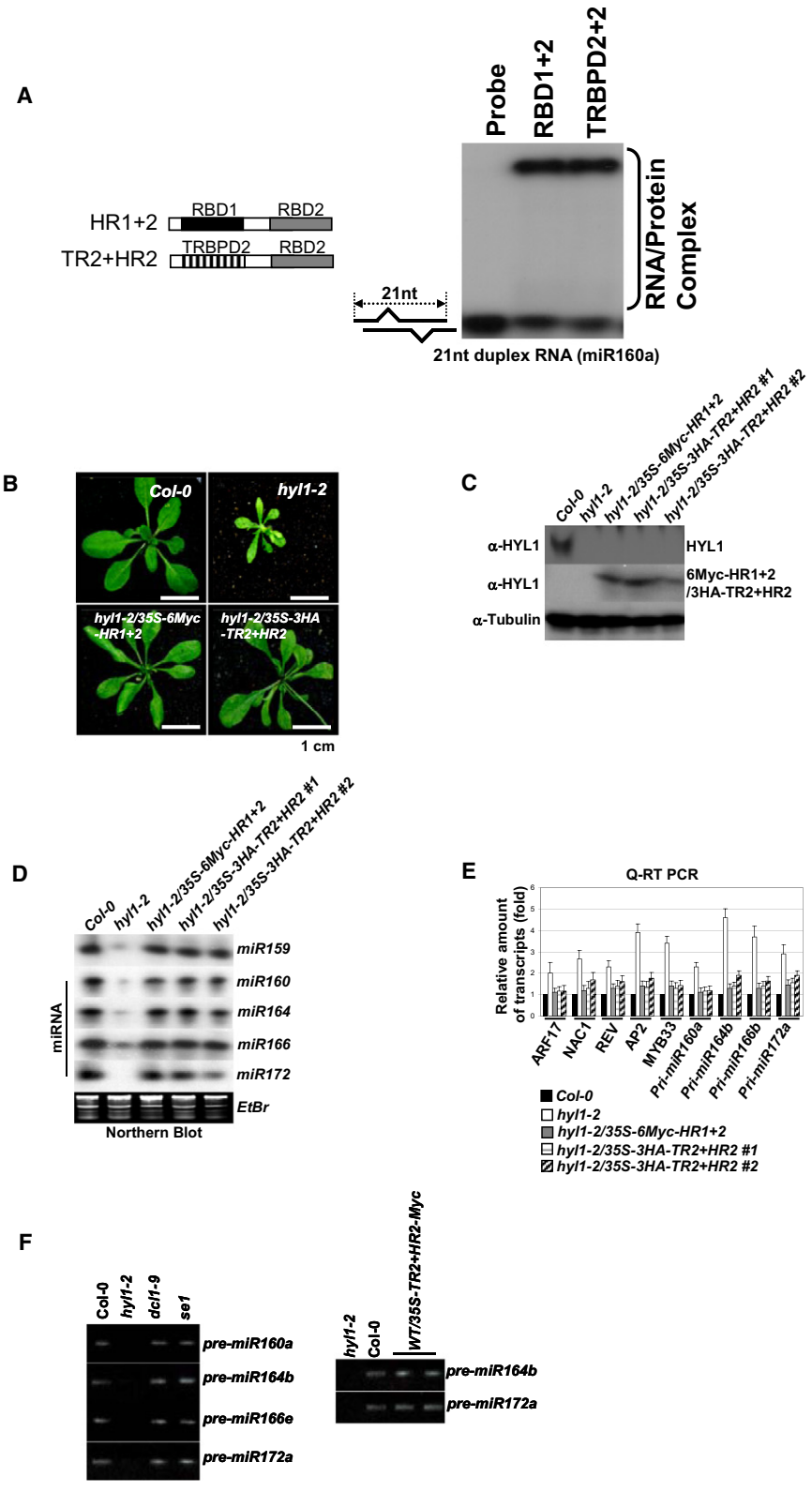

Figure 4. TR2 Can Substitute for HR1 In Vivo and In Vitro

(A) Interaction of HR1+2 and TR2+HR2 with miRNA160/* duplex. (Left) Schematic diagrams of HR1+2 and TR2+HR2 chimeric proteins. Black box represents HR1; gray boxes, HR2; and striped box, TR2. (Right) Gel mobility shift assay of HR1+2 and TR2+HR2. Equal amounts of HYL1 deletion mutant (HR1+2, 2×10^{-8} M) and chimeric protein (TR2+HR2, 2×10^{-8} M) were mixed with 2×10^{-8} M of 21 nt (19 bp duplex) miRNA160/*. HR1+2 and chimeric TR2+HR2 display similar binding affinity.

(B) Overexpression of chimeric protein TR2+HR2 or HR1+2 can rescue the miRNA-deficient phenotype of the *hyl1-2* mutant. Morphology of transgenic lines overexpressing *35-6myc-HR1+2* and *35S-3HA-TR2+HR2* transgenes. Seedlings were grown on soil for 20 days under long day condition.

(C) Protein levels of overexpressed HYL1 dsRBD1+2-6myc and 3HA-TRBPD2+HYL1 dsRBD2. Levels of endogenous HYL1 and transgene products were determined with anti-HYL1 antibody. Tubulin levels were used as a loading control.

(D) Restoration of miRNA levels in *hyl1-2* mutant plants overexpressing *35-6myc-HR1+2* and *35S-3HA-TR2+HR2* transgenes. miRNA levels in transgenic lines *hyl1-2* and WT were analyzed by northern blots. Each lane contained 10 μg of total RNAs. Blots were hybridized to DNA complementary to miRNA159, miRNA160, miRNA164, miRNA166, and miRNA172. 5SRNA/tRNA were used as a loading control.

(E) Levels of target gene transcripts and pri-miRNAs were analyzed by quantitative RT-PCR. Results were normalized with respect to *ACTIN* transcript levels. Average results of three replicates are given along with standard errors.

(F) Detection of miRNA precursors in immunocomplex of HYL1 and/or TR2+HR2. Crude extracts were prepared from WT (Col-0), *se1*, *dcl1-9*, and *hyl1-2* plants and *hyl1-2/35S-3HA-TR2+HR2* transgenic plants. Immunoprecipitations were performed using anti-HYL1 antibody. RNAs in immunocomplex were amplified by PCR using primer pairs to detect miRNA precursors.

(Figure 5C). Determination of the dsRNA amount in the shifted peak gave a HYL1/dsRNA ratio of 2:1, which is consistent with the isothermal titration calorimetry assay (ITC) showing that 21 nt (19 bp duplex) dsRNA harbors two HYL1 binding sites with a binding affinity (Ka) of 2×10^7 (Figure 5D). In order to observe the gradually migration of HYL1/dsRNA complex from a 1:1 ratio to 2:1 ratio, we conducted EMSA using miR160/* as substrate and used gradient gel ranging in polyacrylamide concentration from 15% to ~3.5% to resolve the HYL1/dsRNA complex (instead of 15% as we used for other EMSA experiments). In this condition, we were able to observe complex shifts accompanying the increase of the HYL1 concentration (Figures 5E and 5F). Taken together, our results suggest that HYL1 dimer rather than monomer likely interacts with 21 nt dsRNA.

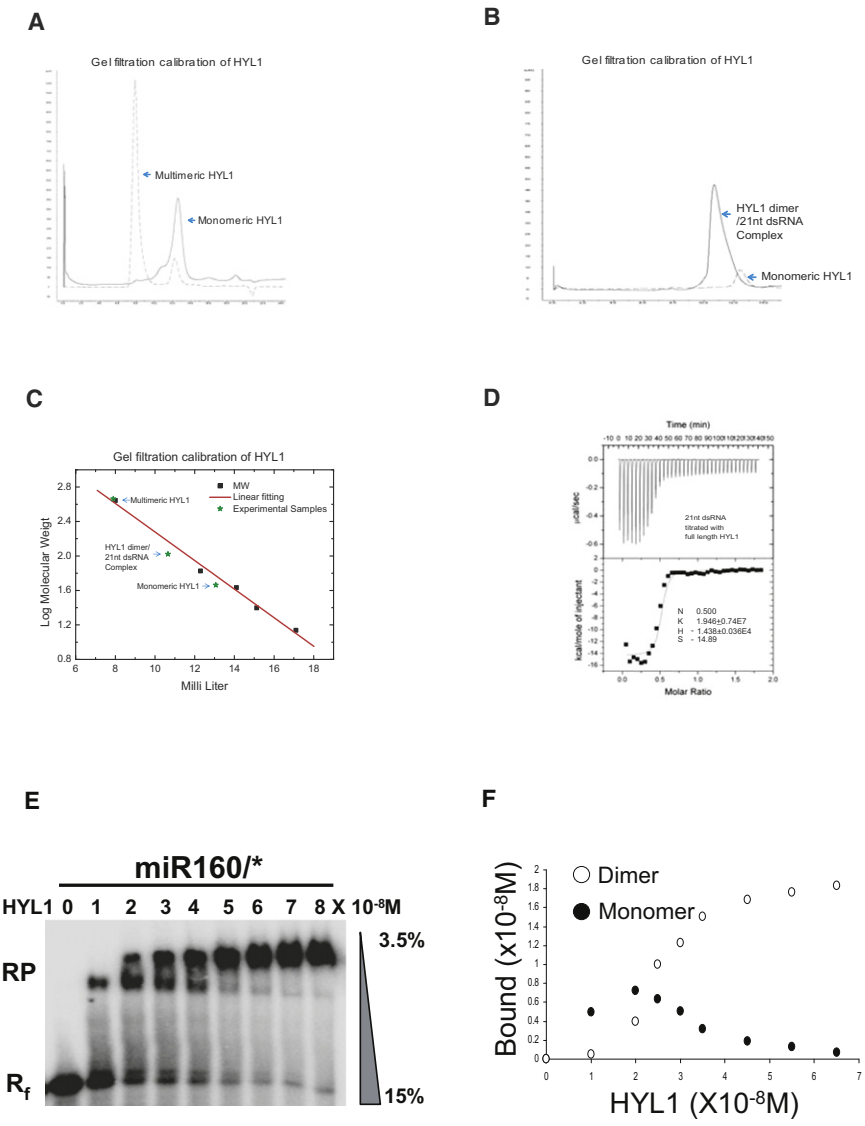

Figure 5. HYL1 Binds to dsRNA as a Dimer

(A) Size fractionation of multimerized HYL1 and monomeric HYL1 without 21 nt dsRNA. Multimerized HYL1 was eluted in high molecular fraction around 440 kDa and monomeric HYL1 was placed between 67 kDa and 43 kDa.

(B) HYL1 dimerization is enhanced by 21 nt dsRNA. Addition of 1.1-fold of 21 nt dsRNA shifted the elution peak of HYL1 to around 110 kDa. HYL1 monomer and HYL1 dimer are indicated.

(C) Molecular mass calculation aligned with the molecular mass markers.

(D) ITC data of HYL1 binding to 21 nt (19 bp duplex) dsRNA. Raw titration data and integrated heat measurements are shown on the top and bottom plots, respectively. The K_d and stoichiometry numbers (n) obtained by fitting a standard two-interaction-site model are shown with standard deviation determined by nonlinear least-square analysis. The n number automatically picked by computer analysis was ~0.48. The K_d value was further recalculated by the fixation of n = 0.5 supported by crystal structure.

(E) Binding of full-length HYL1 to miRNA160/* duplex resolving in gradient gel analysis. Increasing protein concentrations of full-length HYL1 (10^{-8} M to 8 × 10^{-8} M) were added to a fixed amount of 21 nt (19 bp duplex) miRNA160/* (2 × 10^{-8} M). RNA-Protein complex and free RNA were annotated as RP and R_f, respectively.

(F) Bound HYL1 dimer and monomer were calculated from a plot of the fraction bound versus protein concentration.

Next, we performed in vitro pull-down assays to confirm the dimerization capacity of HR2. As expected, GST-HYL1 was able to pull down HR2 but not HR1, whereas addition of 21 nt (19 bp) miR172/* duplex increased the heterodimerization of HYL1 and HR1+2, but an excessive amount of 21 nt (19 bp) miR172/* duplex disrupted their interaction (Figure 6A). These results suggest that an appropriate ratio of dsRNA to protein may facilitate and strengthen HYL1 dimerization. To see whether the heterodimeric interaction can be recapitulated in vivo, we performed coimmunoprecipitation experiments using extracts prepared from plants overexpressing 6Myc-HR1+2. Our results show that the HYL1 antibody indeed detected a band in the immunocomplex containing 6Myc-HR1+2 and the immunocomplex also contained miRNA precursors (Figure 6B).

To investigate whether HYL1 forms a dimer in vivo, we used HYL1 antibody to detect HYL1 from the total protein extract of *Arabidopsis* using different buffer conditions and different extraction procedures. Surprisingly, we were able to detect both HYL1 dimer and monomer using buffer without the addition of SDS and Urea. In contrast, we were only able to detect HYL1 monomer using the buffer in the presence of SDS and Urea (Figure 6C). Moreover, we made a transgenic HA-SERRATE overexpression line to coimmunoprecipitation HYL1 and we were only able to detect HYL1 monomer after extensively washing the coimmunoprecipitation samples with 0.5 M NaCl (Figure 6C). These data suggest that probably additional RNA/protein factors are required for HYL1 dimerization in vivo and strongly support the notion that dsRNA enhances the dimerization of HYL1 in vitro.

DISCUSSION

Proposed Roles of HYL1 in Pri- and Pre-miRNA Processing

Genetic and molecular analyses have shown that accurate processing of pri- and pre-miRNAs in *Arabidopsis* is mediated by a protein complex composed of at least three subunits, DCL1, HYL1, and SE (reviewed by Chen, 2008). As a member of the RNase III family, DCL1 can be safely assumed to play a central role in precursor cleavage, but the precise roles of the other two subunits are poorly understood in molecular terms. Therefore, crystal structures supplemented with functional analysis will pave the way to uncovering the molecular mechanisms on

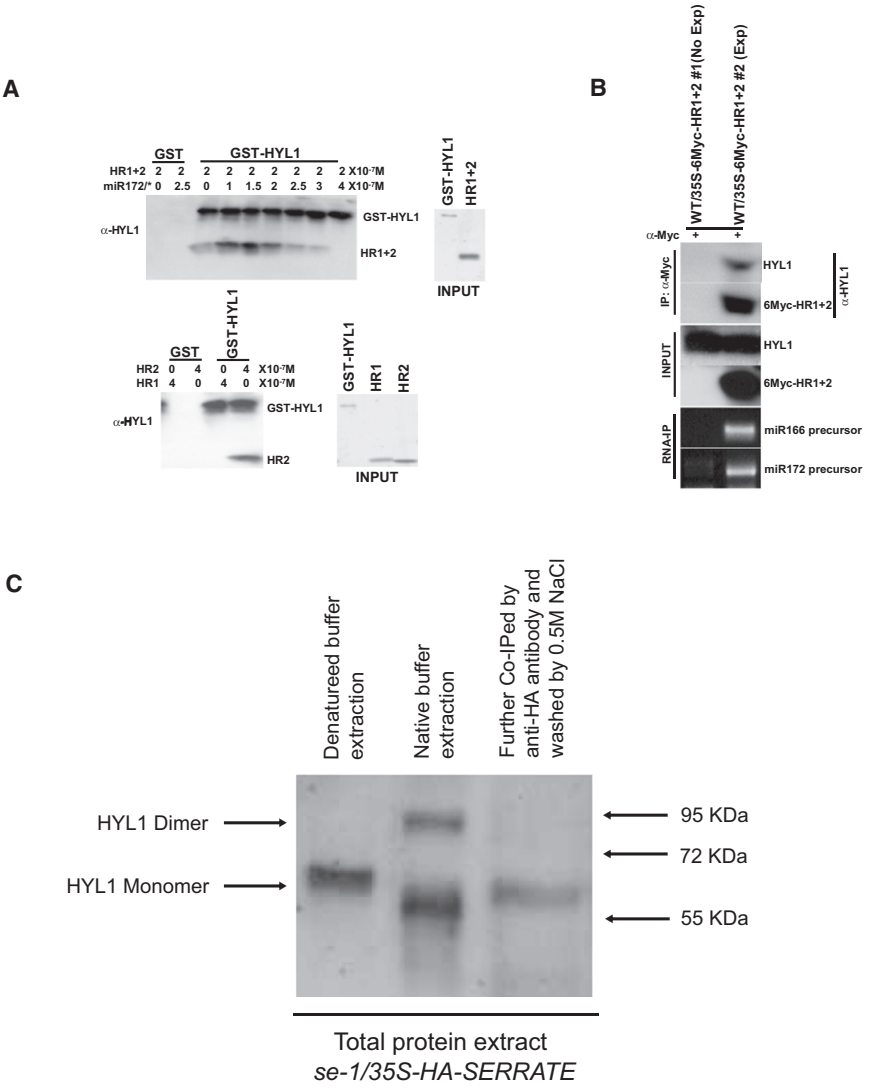

Figure 6. HYL1 Forms Dimer In Vivo

(A) HYL1 interacts with HR1+2 in vitro. (Top) dsRNA miR172/* duplex induces HYL1 and HR1+2 interaction. 0.2 μM of GST-HYL1 was used as bait and incubated with 0.2 μM of HR1+2 and the indicated amount of miR172/*. (Bottom) HR2 domain is responsible for HYL1 dimerization. 0.4 μM of HR1 or HR2 were incubated with 0.2 μM of GST-HYL1 to identify the interaction domain. The amounts of HR1+2, HR1, and HR2 proteins are shown on the INPUT panel. After incubation, GST-HYL1 was retrieved using glutathione beads and pulled down proteins were detected by western blots using antibodies to HYL1.

(B) HYL1 interacts with HR1+2 in vivo. Coimmunoprecipitation of 6Myc-HR1+2 with endogenous HYL1. Seedlings of WT-expressing *35S-6Myc-HR1+2* transgene were used for in vivo interaction analysis. Extracts were treated with anti-Myc antibody and agarose-protein A (50 μl) to immunoprecipitate 6Myc-HR1+2. The immunoprecipitates were analyzed with anti-HYL1 antibody to detect the presence of endogenous HYL1. The non-expressing transgenic *WT/35S-6Myc-HR1+2 #1* line was used as a negative control for coimmunoprecipitation. RNA extracted from immunoprecipitated complex was amplified by PCR using specific primers to miRNA166 and miRNA172 precursors.

(C) HYL1 forms dimer in vivo. (Lane 1) Total *Arabidopsis* protein extracts from HA-SERRATE overexpression lines were treated by "denatured" buffer and detected by anti-HYL1 poly-antibody. (Lane 2) Total *Arabidopsis* protein extracts from HA-SERRATE overexpression lines were treated by "native" buffer and detected by anti-HYL1 poly-antibody. (Lane 3) Total *Arabidopsis* protein extracts from lane 2 were treated with anti-HA antibody and agarose-protein A (50 μl) to immunoprecipitate endogenous HYL1. The immunoprecipitates were analyzed with anti-HYL1 antibody.

miRNA processing (reviewed by Zhu, 2008). Our structural and biochemical analyses on HYL1 shed light on several key features of dsRNA binding and recognition by HYL1. (a) The canonical HR1 shows structural and functional similarity to the canonical TR2 domain of TRBP2 in recognizing dsRNA both in vitro and in vivo. (b) HYL1 forms a functional dimer and the dimerization is probably mediated by HR2 domain. (c) HYL1 recognizes dsRNA in a geometry-dependent but sequence-independent manner. (d) The combination of canonical and noncanonical dsRBDs in tandem is probably the conserved feature for facilitating miRNA processing.

We favor the view that HYL1 may scan through the dsRNA stem portion of miRNA precursors and preferentially binds to the miRNA/miRNA* region. At this moment, we do not know how SE recognizes and enhances the accuracy of pri-miRNA processing. However, HYL1 and SE may work cooperatively as a molecular ruler to recruit DCL1 for pri- and pre-miRNA processing (Figure S5). This working model of HYL1 is consistent with the recent observation that HYL1 and SE together promote accurate processing of pri-miRNA by DCL1 in vitro (Dong et al., 2008) and the report that *hyl1-2* mutant instead of *dcl1-7* or *dcl1-9* mutant displays off-target pri-miRNA cleavage in vivo (Kurihara et al., 2006). This observation further suggests that HYL1 probably binds and protects miRNA/miRNA* region from random slicing by DCL1. A major challenge in the future is to incorporate the important functions of SE and other components of miRNA processing machinery such as DAWDLE (DDL) (Yu et al., 2008) into this model.

Note Added

During the preparation of this manuscript, Tagami et al. (2009) reported that an amino acid substitution of Glu-395 with Lys in the ATPase/DExH-box RNA helicase domain confers restoration of miRNA expression in the *hyl1-2* mutant background (Tagami et al., 2009). This surprising result of the dominant *dcl1-13* mutant seems to imply that HYL1 may not be required for miRNA processing. It is known that the cleavage activity of human Dicer is repressed by its helicase domain and this autoinhibition can be relieved by interaction with TRBP2, which triggers a structural rearrangement of Dicer (Ma et al., 2008). We hypothesize that

a similar situation may apply to the HYL1/DCL1 interaction. HYL1 may have two related functions in miRNA processing. In addition to sensing and protecting the miRNA/miRNA* region within a pri- and pre-miRNA, it may activate the RNase III domain of DCL1 by mediating a structural rearrangement of the latter.

EXPERIMENTAL PROCEDURES

Construction of *Escherichia coli* Expression Vectors and Protein Purification

cDNA encoding full-length HYL1 was cloned in frame into pET29a upstream of DNA sequence encoding 6 histidine. cDNA sequences encoding HYL1 dsRBD1 (HR1; residues 15–84), HYL1 dsRBD2 (HR2; residues 100–172), HYL1 dsRBD1+2 (HR1+2; residues 15–172), HYL1 dsRBD1+2+H (HR1+2+H; residues 15–220), and TRBP2 dsRBD2 (TR2; residues 152–227) were cloned into pET28b downstream of DNA sequences encoding 6 histidine. Chimeric cDNA encoding TRBP2 dsRBD2+HYL1 dsRBD2 (TR2+HR2) was generated by fusing the *TRBP2 dsRBD2* (*TR2*) gene (amplified by primers chimeric-s1 and chimeric-as1 described in Table S1) and the *HYL1 dsRBD2* (*HR2*) gene (amplified by primers chimeric-s2 and chimeric-as2) by overlapping PCR and cloned into pET28b downstream of DNA sequence encoding 6 histidine. The fusion gene encoding glutathionin-S-transferase (GST) fused to HYL1 was prepared using pGEX-4T-1 vector. Mutants of full-length HYL1 were prepared using the QuikChange Site-Directed Mutagenesis Kit (Stratagene) and the constructs were verified by sequencing.

For protein expression, transformed *E. coli* cells were grown to an OD600 of ~0.6 and induced overnight at 20°C using 0.4 mM isopropyl β-d-thiogalactoside. After centrifugation, cells were resuspended in 1 mM EDTA, 1 mM dithiothreitol (DTT), complete proteinase inhibitor (Roche), 1.0 M NaCl, and 50 mM Tris (pH 7.4) and lysed by cell disruptor. After centrifugation (40,000 × g, 1 hr), the supernatant was loaded onto a Ni^{2+} affinity column that was equilibrated in 50 mM Tris (pH 7.6) with 500 mM NaCl. Nonspecific-binding proteins were washed out by the same buffer with 25 mM imidazole, and specific-binding protein was eluted with 250 mM imidazole in the same buffer. Pooled fractions from the Ni^{2+} affinity column were concentrated and then purified on a HiLoad Superdex S-75 26/60 column (Amersham) equilibrated in 500 mM NaCl, 10 mM DTT, and 25 mM Tris (pH 7.4). The purified protein was concentrated to 10 mg/ml in a Microcon (Amicon) and then dialyzed against 50 mM NaCl. 21 nt RNA oligoribonucleotides were purchased from Dharmacon. GST-fused HYL1 was purified with glutathione Sepharose resin (GE Healthcare).

Crystallization and Data Collection

Crystals of HR1, HR2, HR1/dsRNA complex, and TR2/dsRNA complex were grown by hanging drop vapor diffusion at 20°C. Typically, a 2 μl hanging drop contained 1.0 μl of protein or protein-RNA complex (0.4 mM) mixed with 1.0 μl of reservoir solution and equilibrated over 1 ml of reservoir solution. HR1 crystals grew to a maximum size of 0.20 mm × 0.10 mm × 0.10 mm over the course of 2 days under the crystallization condition of 35% PEG 400, 0.2 M magnesium chloride, and 100 mM HEPES (pH 7.5). HR2 crystals grew to a maximum size of 0.15 mm × 0.02 mm × 0.02 mm over the course of 14 days under the crystallization condition of 28% PEG 400, 0.2 M calcium chloride, and 100mM HEPES (pH 7.5). HR1/dsRNA complex was prepared by annealing RNA1 and RNA2 first and then incubating the RNA duplex with HR1 for 20 min before crystallization. The HR1/dsRNA complex crystals grew to a maximum size of 0.15 mm × 0.02 mm × 0.02 mm over the course of 3 days under the crystallization condition of 30% PEG 8000, 0.2 M ammonium sulfate, and 100 mM sodium cacodylate (pH 7.5). TR2/dsRNA complex was prepared by incubating GC10 RNA with TRBP2 dsRBD2 for 20 min before crystallization. TR2/dsRNA complex crystals grew to a maximum size of 0.15 mm × 0.05 mm × 0.05 mm over the course of 2 days under the crystallization condition of 2.0 M ammonium sulfate, 10 mM magnesium sulfate, and 0.05M sodium cacodylate (pH 6.5).

For data collection, crystals were flash frozen (100 K) in the above reservoir solution (HR1) or had increased PEG 400 to 35% (HR2) or were supplemented with 30% glycerol (HR1/dsRNA and TR2/dsRNA). HR1 data, HR2 data, and HR1/dsRNA data were collected at 1.5418 Å on our in-house Rigaku diffractometer. A total of 150 frames of 1° oscillation were collected for HR1; a total of 180 frames of 1° oscillation were collected for HR2; a total of 180 frames of 1° oscillation were collected for HR1/dsRNA. TR2 data set was collected at 1.1Å on beamline X12C at the National Synchrotron Light Source at Brookhaven National Laboratory. A total of 360 frames of 1° oscillation were collected. All data sets were processed by HKL2000 (www.hkl-xray.com). The crystals belonging to space group $P2_12_12_1$ (HR1), $P4_3$ (HR2), $P4_3$ (HR1/dsRNA), and $I2_12_12_1$ (TR2/dsRNA) with unit cell parameters are listed in Table 1.

Structure Determination

Crystal structures of HR1, HR2, HR1/dsRNA complex, and TR2/dsRNA complex were determined by molecular replacement using the crystal structure of the second dsRBD of *Xenopus laevis* RNA-binding protein A as the search model (PDBID: 1DI2). Models were rebuilt by using the program O (Jones et al., 1991) and refined using REFMAC/CCP4 (CCP4, 1994) with R_{work} = 20.7% and R_{free} = 25.4% (HR1), R_{work} = 25.5% and R_{free} = 32.2% (HR2), R_{work} = 20.4% and R_{free} = 31.7% (HR1/dsRNA complex), and R_{work} = 26.1% and R_{free} = 29.8% (TR2/dsRNA complex). The R free set contained 5% or 10% (HR2) of the reflections chosen at random.

Plant Material, Growth Conditions, and Generation of Transgenic Plants

The *hyl1-2* (SALK_064863) mutant and all transgenic lines used are in the Col-0 background. Sterilized seeds were germinated on MS medium with 1% sucrose. After 4 days of incubation in darkness at 4°C, seeds were incubated at 22°C under long day light condition. Plants were transformed by *Agrobacterium* (EHA105 strain)-mediated infiltration using the floral dip method (Clough and Bent, 1998; Zhang et al., 2006a).

Production of Overexpression Lines

35S-HYL1-6Myc, *35S-6Myc-HR1+2*, and *35S-3HA-TR2+HR2* transgenes were constructed using pBA002-6myc and pBA002-3HA binary vectors. PCR product for HR1+2 DNA fragment was generated by XhoIHYL1 dsRBD-s and AscIHYL1 dsRBD2-as primers and inserted into pBA002-6myc binary vectors. *35S-HA-SERRATE* transgene was constructed using pBA002-3HA binary vector. For construction of the TR2+HR2 chimeric gene, the chimeric DNA fragment used for protein expression was amplified by AvrIIHYL1 dsRBD1 s and PacIHYL1 dsRBD2-as primers and subcloned into pBA002-3HA binary vector (Table S1). Constructs were transferred into WT or *hyl1-2* mutant to generate *hyl1-2/35S-HYL1-6Myc*, *WT/35S-6Myc-HR1+2*, *hyl1-2/35S-6Myc-HR1+2*, and *hyl1-2/35S-3HA-TR2+HR2* transgenic lines.

RNA Extraction, RT-PCR, QRT-PCR, and Northern Blot Hybridization

Total RNA was extracted from *Arabidopsis* seedlings using RNeasy Plant Mini kits (QIAGENe) or Trisol reagent (Invitrogen). Reverse transcription was performed using Ready-To-go You Prime First Strand Beads (GE Healthcare) or MMLV reverse transcriptase system (Promega) according to the manufacturer's instruction. QRT-PCR was performed with Applied Biosystems 7900HT real-time PCR system using the oligonucleotides described in Table S1. Relative amounts of target genes were calculated by the formula $2^{(-\Delta\Delta CT)}$, where C_T was the cycle number at which the fluorescence reached the threshold point for detection. All calculations were calibrated by *ACTIN* threshold cycles with three individual replicates to reduce loading errors. MiRNA northern blot analysis was performed as described in Zhang et al. (2006b) using complementary DNA sequences for miR159, miR160, miR164, miR166, and miR172 (Table S1). For western blot analysis, seedlings were ground with Tissuelyzer (QIAGENe) in 6× SDS-sample buffer for 1 min. Samples were then incubated at 100°C for 10 min and extracts were resolved on 10% SDS-PAGE gels. Blots were detected with anti-HYL1 antibodies and anti-tubulin antibodies.

Gel Shift Mobility Assays

^{32}P-UTP-labeled pri-miRNA164b RNA and pre-miRNA164b probes were produced by in vitro transcription kits (Ambion) following the manufacturer's instructions. Short RNA probes for gel mobility shift assay were labeled with ^{32}P-ATP and the sequences were given in Table S1. Concentration of RNA probes and proteins are described in the figure legends. Reaction mixtures

were incubated at 4°C for 30 min and resolved on TBE (pH 6.5–8.0)- or Tris-Cl (pH 8.0)-buffered 4%–15% polyacrylamide gel with Tris-Cl (pH 7.4–8.0)-buffered 4%–8% stacking polyacrylamide gel at 4°C or 22°C. To compare the binding affinity among different deletion constructs, a fixed amount of 21 nt (19 bp duplex) miRNA160/* (2×10^{-8}M) probes was titrated with increasing amount of proteins: HYL1 (5×10^{-9} M to 3.2×10^{-7} M), HR1+2 (1×10^{-8} M to 5.5×10^{-7} M), TR2+HR2 (1×10^{-8} M to 5.5×10^{-7} M), and HR1 (2×10^{-7} M to 6×10^{-5} M). Data were analyzed using the equation $[RNA_{bound}]/[RNA_{total}] = [Protein]/(K_d + [Protein])$ and apparent dissociation constants were calculated by fitting the saturation hyperbola graphs from fraction bound (F) versus protein concentration (P), where $F = [RNA_{bound}]/[RNA_{total}]$.

In Vitro Pull-Down Assays

GST-HYL1 fusion protein (2×10^{-7}M) was applied to 1 ml of binding buffer [50 mM Tris-HCl (pH 7.4), 100 mM NaCl, 0.6% Triton X-100, and 50 U/ml RNAsin] with HR1+2 (2×10^{-7} M), $HR1^{1-100}$(4×10^{-7} M), and $HR2^{101-171}$ (4×10^{-7} M) and incubated with or without 21 nt (19 bp duplex) miRNA172/* (0 to 4×10^{-7} M). Reaction mixtures were incubated with 30 μl of 70% glutathione-S-transferase bead at 4°C for 2 hr and extensively washed with binding buffer containing 1% Triton X-100. Samples were boiled at 100°C with 6× SDS-sample buffer and resolved by 8% of SDS-PAGE. Resolved proteins were transferred to PVDF membrane and western blots were analyzed using anti-HYL1 antibody.

HYL1 Dimer Detection In Vivo

The flower clusters (~0.1g) were collected from HA-SERRATE overexpression line 5–7 weeks old, frozen in liquid nitrogen, and homogenized in 0.7 ml of "native" buffer [25 mM Tris (pH 7.4), 25 mM potassium phosphate (pH 6.8), 500 mM NaCl, 10% glycerol, and 1 mM DTT] supplemented with 2% β-mercaptoethanol and proteinase inhibitor cocktail or "denatured" buffer [50 mM Tris (pH 6.8), 4.5% SDS, 7.5% β-mercaptoethanol, and 9 M Urea], respectively. After separation from insoluble fractions by centrifuge, the extract was incubated with EZview Red anti-HA Affinity Gel (Sigma-Aldrich) for 1 hr at 4C°, washed with "native" buffer, and eluted as described in the manufacturer's instructions. The eluent was resolved by 12% SDS-PAGE and detected by western blot using polyclonal antibodies raised in rabbit against SERRATE and HYL1.

Coimmunoprecipitation of Pri-miRNA and Pre-miRNA

WT (Col-0), *hyl1-2*, *dcl1-9*, *se1*, and *hyl1-2/35S-3HA-TR2+HR2* lines were subjected to in vivo crosslinking and immunoprecipitation using the modified method of Song et al. (2007). Coimmunoprecipitated pri-miRNAs and pre-miRNAs were detected by PCR using primers in Table S1. Coimmunoprecipitation of endogenous HYL1 was performed with *WT/35S-6Myc-HR1+HR2* lines as described by Jang et al. (2007).

Analytical Gel Filtration

Full-length HYL1 protein and protein-RNA complexes were analyzed on a Superdex 200 10/300 GL column with a flow rate of 0.5 ml/min with an injection volume of 0.1 ml. All experiments were performed in a buffer of 25 mM Tris-HCl and 100 mM NaCl (pH 7.4). For the complex, HYL1 was incubated with 21 nt dsRNA duplex at a molar ratio of (1:1.1) on ice for 1 hr. The column was first calibrated with the high molecular weight gel filtration kit (GE Healthcare) and the corresponding curves were established by OriginPro 7.5.

Isothermal Titration Calorimetry Assay

All experiments were performed in a buffer containing 12.5 mM Tris-HCl (pH 7.4) and 100 mM NaCl. Full-length HYL1 (20 μM) and 21 nt (19 bp duplex) dsRNA duplex (200 μM) samples were filtered and degassed before titration. Protein sample was loaded into the cell and RNA sample was loaded into the syringe with a stirring speed of 310 rpm (Microcal VP-ITC calorimeter). Data were collected in the high feedback mode with a filter period of 3 s. The calorimetric data were processed and fitted into the single set of identical sites model using Microcal Origin (Version 5.0) and analyzed by the software supplied by the instrument.

ACCESSION NUMBERS

Sequence data from this article can be found in the *Arabidopsis* Genome Initiative or GenBank/EMBL databases under the following accession numbers: HYL1(AT1G09700), ARF17(AT1G77850), REV(AT5G60690), NAC1(AT1G56010), and AP2(AT4G36920). Coordinates and structure factors have been deposited to Protein Data Bank with accession numbers 3ADG (HR1), 3ADI (HR1/dsRNA), 3ADJ (HR2), and 3ADL (TR2/dsRNA).

SUPPLEMENTAL INFORMATION

Supplemental Information includes five figures and two tables and can be found with this article online at doi:10.1016/j.str.2010.02.006.

ACKNOWLEDGMENTS

We thank A. Saxena at X12C at the National Synchrotron Light Source of the Brookhaven National Laboratory for assistance with data collection. This work was supported by intramural research funds from Temasek Life Sciences Laboratory, National University of Singapore Research Scholarship, and Singapore Ministry of Education (T208A3124 to Y.A.Y.). Work performed at the Rockefeller University was supported by National Institutes of Health grant GM44640 to N.-H.C. S.W.Y. performed biochemical and genetic analyses; H.-Y.C. performed constructs screening, subcloning, and protein crystallization; J.Y. performed ITC and gel filtration analysis; S.M. performed HYL1 dimer detection; and Y.A.Y. solved the structures. Y.A.Y., S.W.Y., and N.-H.C. wrote the paper with input from H.-Y.C.

Received: September 16, 2009
Revised: January 23, 2010
Accepted: February 9, 2010
Published: May 11, 2010

REFERENCES

CCP4 (Collaborative Computational Project, Number 4). (1994). The CCP4 suite: programs for protein crystallography. Acta Crystallogr. D Biol. Crystallgr. *50*, 760–763.

Chen, X. (2008). MicroRNA metabolism in plants. Curr. Top. Microbiol. Immunol. *320*, 117–136.

Chendrimada, T.P., Gregory, R.I., Kumaraswamy, E., Norman, J., Cooch, N., Nishikura, K., and Shiekhattar, R. (2005). TRBP recruits the Dicer complex to Ago2 for microRNA processing and gene silencing. Nature *436*, 740–744.

Clough, S.J., and Bent, A.F. (1998). Floral dip: a simplified method for Agrobacterium-mediated transformation of Arabidopsis thaliana. Plant J. *16*, 735–743.

Collins, R.E., and Cheng, X. (2005). Structural domains in RNAi. FEBS Lett. *579*, 5841–5849.

Daviet, L., Erard, M., Dorin, D., Duarte, M., Vaquero, C., and Gatignol, A. (2000). Analysis of a binding difference between the two dsRNA-binding domains in TRBP reveals the modular function of a KR-helix motif. Eur. J. Biochem. *267*, 2419–2431.

Dong, Z., Han, M.H., and Fedoroff, N. (2008). The RNA-binding proteins HYL1 and SE promote accurate in vitro processing of pri-miRNA by DCL1. Proc. Natl. Acad. Sci. USA *105*, 9970–9975.

Doyle, M., and Jantsch, M.F. (2002). New and old roles of the double-stranded RNA-binding domain. J. Struct. Biol. *140*, 147–153.

Förstemann, K., Tomari, Y., Du, T., Vagin, V.V., Denli, A.M., Bratu, D.P., Klattenhoff, C., Theurkauf, W.E., and Zamore, P.D. (2005). Normal microRNA maturation and germ-line stem cell maintenance requires Loquacious, a double-stranded RNA-binding domain protein. PLoS Biol. *3*, e236.

Grigg, S.P., Canales, C., Hay, A., and Tsiantis, M. (2005). SERRATE coordinates shoot meristem function and leaf axial patterning in Arabidopsis. Nature *437*, 1022–1026.

Han, J., Lee, Y., Yeom, K.H., Kim, Y.K., Jin, H., and Kim, V.N. (2004a). The Drosha-DGCR8 complex in primary microRNA processing. Genes Dev. *18*, 3016–3027.

Han, M.H., Goud, S., Song, L., and Fedoroff, N. (2004b). The Arabidopsis double-stranded RNA-binding protein HYL1 plays a role in microRNA-mediated gene regulation. Proc. Natl. Acad. Sci. USA *101*, 1093–1098.

Han, J., Lee, Y., Yeom, K.H., Nam, J.W., Heo, I., Rhee, J.K., Sohn, S.Y., Cho, Y., Zhang, B.T., and Kim, V.N. (2006). Molecular basis for the recognition of primary microRNAs by the Drosha-DGCR8 complex. Cell *125*, 887–901.

Hutvágner, G., and Simard, M.J. (2008). Argonaute proteins: key players in RNA silencing. Nat. Rev. Mol. Cell Biol. *9*, 22–32.

Hutvágner, G., McLachlan, J., Pasquinelli, A.E., Bálint, E., Tuschl, T., and Zamore, P.D. (2001). A cellular function for the RNA-interference enzyme Dicer in the maturation of the let-7 small temporal RNA. Science *293*, 834–838.

Jang, I.C., Yang, S.W., Yang, J.Y., and Chua, N.H. (2007). Independent and interdependent functions of LAF1 and HFR1 in phytochrome A signaling. Genes Dev. *21*, 2100–2111.

Jaskiewicz, L., and Filipowicz, W. (2008). Role of Dicer in posttranscriptional RNA silencing. Curr. Top. Microbiol. Immunol. *320*, 77–97.

Ji, X. (2008). The mechanism of RNase III action: how dicer dices. Curr. Top. Microbiol. Immunol. *320*, 99–116.

Jiang, F., Ye, X., Liu, X., Fincher, L., McKearin, D., and Liu, Q. (2005). Dicer-1 and R3D1-L catalyze microRNA maturation in Drosophila. Genes Dev. *19*, 1674–1679.

Jinek, M., and Doudna, J.A. (2009). A three-dimensional view of the molecular machinery of RNA interference. Nature *457*, 405–412.

Jones, T.A., Zou, J.Y., Cowan, S.W., and Kjeldgaard, G.J. (1991). Improved methods for building protein models in electron density maps and the location of errors in these models. Acta Crystallogr. A *47*, 110–119.

Kurihara, Y., Takashi, Y., and Watanabe, Y. (2006). The interaction between DCL1 and HYL1 is important for efficient and precise processing of pri-miRNA in plant microRNA biogenesis. RNA *12*, 206–212.

Landthaler, M., Yalcin, A., and Tuschl, T. (2004). The human DiGeorge syndrome critical region gene 8 and its D. melanogaster homolog are required for miRNA biogenesis. Curr. Biol. *14*, 2162–2167.

Liu, Q., Rand, T.A., Kalidas, S., Du, F., Kim, H.E., Smith, D.P., and Wang, X. (2003). R2D2, a bridge between the initiation and effector steps of the Drosophila RNAi pathway. Science *301*, 1921–1925.

Lobbes, D., Rallapalli, G., Schmidt, D.D., Martin, C., and Clarke, J. (2006). SERRATE: a new player on the plant miRNA scene. EMBO Rep. *7*, 1052–1058.

Lu, C., and Fedoroff, N. (2000). A mutation in the Arabidopsis HYL1 gene encoding a dsRNA binding protein affects responses to abscisic acid, auxin, and cytokinin. Plant Cell *12*, 2351–2366.

Ma, E., MacRae, I.J., Kirsch, J.F., and Doudna, J.A. (2008). Autoinhibition of human dicer by its internal helicase domain. J. Mol. Biol. *380*, 237–243.

Ramos, A., Grünert, S., Adams, J., Micklem, D.R., Proctor, M.R., Freund, S., Bycroft, M., St Johnston, D., and Varani, G. (2000). RNA recognition by a Staufen double-stranded RNA-binding domain. EMBO J. *19*, 997–1009.

Ryter, J.M., and Schultz, S.C. (1998). Molecular basis of double-stranded RNA-protein interactions: structure of a dsRNA-binding domain complexed with dsRNA. EMBO J. *17*, 7505–7513.

Saito, K., Ishizuka, A., Siomi, H., and Siomi, M.C. (2005). Processing of pre-microRNAs by the Dicer-1-Loquacious complex in Drosophila cells. PLoS Biol. *3*, e235.

Siomi, H., and Siomi, M.C. (2009). On the road to reading the RNA-interference code. Nature *457*, 396–404.

Sohn, S.Y., Bae, W.J., Kim, J.J., Yeom, K.H., Kim, V.N., and Cho, Y. (2007). Crystal structure of human DGCR8 core. Nat. Struct. Mol. Biol. *14*, 847–853.

Song, L., Han, M.H., Lesicka, J., and Fedoroff, N. (2007). Arabidopsis primary microRNA processing proteins HYL1 and DCL1 define a nuclear body distinct from the Cajal body. Proc. Natl. Acad. Sci. USA *104*, 5437–5442.

Tagami, Y., Motose, H., and Watanabe, Y. (2009). A dominant mutation in DCL1 suppresses the hyl1 mutant phenotype by promoting the processing of miRNA. RNA *15*, 450–458.

Tomari, Y., Matranga, C., Haley, B., Martinez, N., and Zamore, P.D. (2004). A protein sensor for siRNA asymmetry. Science *306*, 1377–1380.

Tomari, Y., Du, T., and Zamore, P.D. (2007). Sorting of Drosophila small silencing RNAs. Cell *130*, 299–308.

Wu, F., Yu, L., Cao, W., Mao, Y., Liu, X., and He, Y. (2007). The N-terminal double stranded RNA binding domains of Arabidopsis HYPONASTIC LEAVES1 are sufficient for pre miRNA processing. Plant Cell *19*, 914–925.

Yu, B., Bi, L., Zheng, B., Ji, L., Chevalier, D., Agarwal, M., Ramachandran, V., Li, W., Lagrange, T., Walker, J.C., and Chen, X. (2008). The FHA domain proteins DAWDLE in Arabidopsis and SNIP1 in humans act in small RNA biogenesis. Proc. Natl. Acad. Sci. USA *105*, 10073–10078.

Zhang, X., Henriques, R., Lin, S.S., Niu, Q.W., and Chua, N.H. (2006a). Agrobacterium-mediated transformation of Arabidopsis thaliana using the floral dip method. Nat. Protoc. *1*, 641–646.

Zhang, X., Yuan, Y.R., Pei, Y., Lin, S.S., Tuschl, T., Patel, D.J., and Chua, N.H. (2006b). Cucumber mosaic virus-encoded 2b suppressor inhibits Arabidopsis Argonaute1 cleavage activity to counter plant defense. Genes Dev. *20*, 3255–3268.

Zhu, J.K. (2008). Reconstituting plant miRNA biogenesis. Proc. Natl. Acad. Sci. USA *105*, 9851–9852.